Core electrons and specific heat capacity in the fast electron heating of solids

A.P.L. Robinson and J. Pasley

Published Version Information

Citation: APL Robinson and J Pasley. "Core electrons and specific heat capacity in the fast electron heating of solids." Physics of Plasmas, vol. 27, no. 7 (2020): 072701.

DOI: 10.1063/5.0007357

Core Electrons and Specific Heat Capacity in the Fast Electron Heating of Solids.

A.P.L.Robinson[1, a)] and J.Pasley[2]
[1)] *Central Laser Facility, STFC Rutherford-Appleton Laboratory, Didcot, OX11 0QX, United Kingdom*
[2)] *York Plasma Institute, University of York, York, YO10 5DD, United Kingdom*

(Dated: 29 May 2020)

The accuracy with which the Thomas-Fermi (TF) model can provide electronic specific heat capacities for use in calculations relevant to fast electron transport in laser-irradiated solids is examined. It is argued that the TF model, since it neglects quantum shell structure, is likely to be significantly inaccurate for low- and intermediate-Z materials. This argument is supported by examining the results of calculations using more sophisticated methods that account for both degeneracy, quantum shell structure, and other non-ideal corrections. It is further shown that the specific heat capacity curve generated by this more advanced treatment leads to substantial (factor of two) changes in fast electron transport simulations relative to similar modelling based upon the TF model.

I. INTRODUCTION

In this paper the role of the specific heat capacity in the fast electron heating of solids is interrogated. It is well known that multi-MeV suprathermal electrons are generated when ultra-intense ($I\lambda^2 > 10^{18}$ Wcm$^{-2}\mu m^2$) ps-duration lasers irradiate solids[1–4]. These interactions produce current densities in excess of 10^{15} Am^{-2} , which results in violent heating, driven by the return current, on a sub-picosecond timescale. The ability to heat high-density materials with lasers in this fashion has sparked considerable interest in using such a heat source in advanced inertial fusion concepts[5–8]. This heating mechanism is also of interest as regards investigating the properties of both warm[9–11] and hot dense matter[12,13].

Using existing high-energy, high-intensity, laser systems, the peak temperatures that are achieved in a solid-density material via hot-electron driven return current heating, is in the range ~ 300 eV to ~ 1keV, dependant upon the laser and target parameters[14]. The temperatures produced are however significantly non-uniform, due to the strong spreading of the beam due to intrinsic angular spread[15–19], meaning that a broad temperature distribution is generated rather than efficient heating of a volumetrically limited region, such as would be ideal from the standpoint of fusion and other applications. There have been a number of theoretical and experimental efforts to improve the guiding of fast electrons[20–25]. These studies suggest that, using such guiding techniques, it is possible to heat a target in a more controlled fashion. This may be done either with the aim of achieving a higher peak temperature or of raising a larger volume to temperatures that were already achievable, depending on what is required in a given application.

For most low- to intermediate-Z solids this means that the hottest regions consist of He-like or even H-like ions. Since the ionization energies of the innermost shells exceed 100eV for most of these elements, care has to be taken into accounting for the effect of ionization on the energy balance of the background plasma. This suggests that there is the potential to create substantial errors in the electronic specific heat capacity, and therefore that some care needs to be taken in choosing a specific heat capacity model for a given problem.

Here we consider a popular model, used in many numerical simulations of fast electron transport: the Thomas-Fermi (TF) model. We compare this to both classical and non-ideal Saha models for the specific case of solid carbon. This comparison indicates that there are probably issues with the Thomas-Fermi model in the relatively high temperature regime due to the TF model neglecting quantum shell structure (Section II). We argue that a better treatment of the limitations put on heating by ionization may be achieved by using a thermodynamic approach to calculate the specific heat capacity (Section III). The consequences of this for modelling fast electron propagation in solids irradiated by ultra-intense laser pulses are then examined. It is shown that using the TF model can lead to a peak magnetic flux density being calculated that is as much as two times smaller than the flux densities predicted by the same code using a more sophisticated model for the specific heat capacity.

II. THEORY

In a weakly-coupled plasma, the composition can be calculated from the Saha equation[26]. This gives a set of coupled equations at a given temperature. Since the assumption of weak coupling implies an ideal Equation of State (EOS) for the free particles, the results of solving the Saha equations can be used to determine the internal energy, pressure, and the specific heat capacity.

In laser-plasma studies, plasmas will not, in general, be weakly coupled. Inter-particle interactions and correlations will lead to a non-Ideal EOS and plasma compo-

[a)] Electronic mail: alex.robinson@stfc.ac.uk (corresponding author)

sition. The Ionization Potential Depression (IPD) can be a strong effect[27]. The electrons can also be degenerate.

For these reasons, the Thomas-Fermi (TF) model[28] has been a particularly popular model for laser-plasma modelling, including in fast electron transport. The model incorporates both degeneracy and plasma correlation effects, but is best described as "semi-classical". The main weakness of the TF model is that it does not properly account for a number of quantum mechanical effects such as atomic shell structure and energy quantization, and this weakness has been problematic, particularly in regards to calculating EOS[29–33]. To be clear : electron-ion attraction is incorporated into the TF model[26,28], but shell structure is not reproduced by the model.

Firstly the relevance of these effects across the temperature range of interest is examined. This is done for carbon at 2 g/cc.

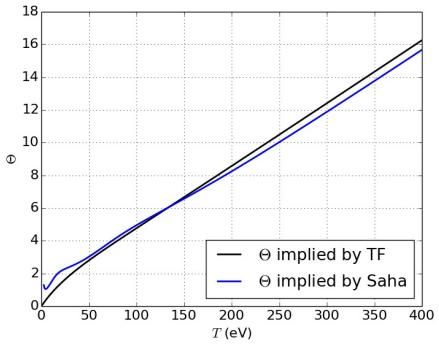

FIG. 1. Plot of the degeneracy parameter, Θ, in solid density carbon.

Fig. 1 shows the degeneracy parameter, $\Theta = k_B T/E_F$ plotted for carbon from 1 to 400eV using the electron density determined by both classical Saha and the TF model. From this it is apparent that for T > 75eV, the plasma is essentially non-degenerate.

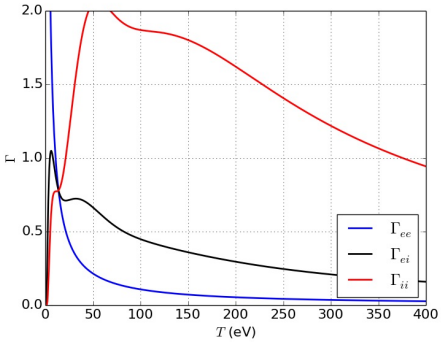

FIG. 2. Coupling parameters in solid density carbon.

Fig. 2 shows the electron-electron, electron-ion, and the ion-ion coupling parameters calculated using values of $Z^\star$ determined by the TF model. This shows that above 75eV, the electron-electron and electron-ion coupling is either moderate or weak. Overall, based on these considerations, the parameters suggest that strong coupling and degeneracy are important below about 75eV, but should become increasingly weak as one moves above this temperature, and thus using the Saha model as a point of comparison above this temperature should not be grossly misleading. A reminder of the classical Saha formulae is given in Appendix A.

Now we shall examine the differences between the TF and classical Saha models themselves. For the Saha model we have solved the Saha system numerically using a multivariate Newton-Raphson method. For the TF model we have used More's fitting formula for $Z^\star$[26], and Bell's fitting formula for the Specific Heat Capacity. Fig. 3 shows $Z^\star$ as determined by each model.

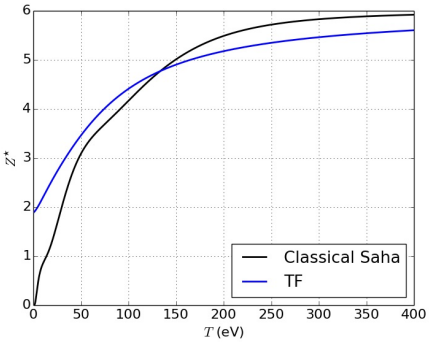

FIG. 3. Plot of $Z^\star$ in TF and Saha model (see text).

In both models the SHC can be expressed as $\partial U/\partial T = Cen_i$, and thus the behaviour of the SHC is completely expressed by C alone. In an ideal, fully ionized plasma we expect $C = 3Z/2$, and thus C should asymptotically approach this limit in both models. In fig. 4 we show the SHC as determined by each model expressed in terms of C alone.

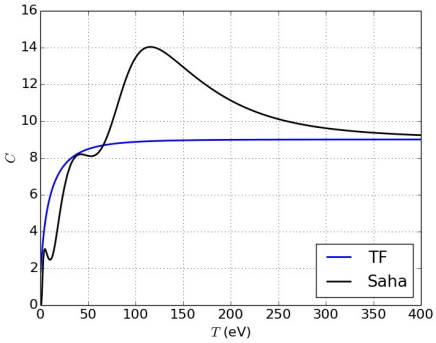

FIG. 4. Plot of the Specific Heat Capacity in terms of C as predicted by the TF model and Saha model for solid density carbon.

While the differences in $Z^\star$ are not dramatic, the differences in the SHC are clearly significant. The largest differences manifest at moderate to high temperatures ($>$ 50eV), in the region where the SHC predicted by the classical Saha model is maximised. Given that the differences in SHC between the two models range up to 55%, there are reasons to be concerned about the accuracy of the TF model in the case of solid carbon. Although the Saha model cannot be expected to be a 'good' model for the ionization, there are two factors to consider. Firstly the behaviour of the Saha model at high temperature will be controlled by the last ionization stages of carbon. Since the TF model is known to neglect quantum shell structure, large discrepancies between the two models in this temperature range are most likely symptomatic of this, leading the TF to be inaccurate in this problem. Secondly, in the high temperature range, $\Theta > 4$, the lack of quantum statistics does not present a difficulty for the Saha model.

It is therefore reasonable to ask if the Saha model could be brought into agreement with the TF model by incorporating Ionization Potential Depression (IPD). The largest IPD that we might reasonably expect in this regime is that predicted by the Ion Sphere model[28],

$$\Delta I_{IS} = \frac{3}{2}\frac{ze^2}{4\pi\varepsilon_0 r_s} \quad (1)$$

where r_s is the ion sphere radius, and z is the charge state of a specific ion. For $z = 6$, this yields ΔI_{IS} =97eV. Suppose that this is applied *uniformly* to the Saha equation, i.e. all ionization receive this IPD, and ionization states are eliminated if the ionization energy is reduced to zero or less.

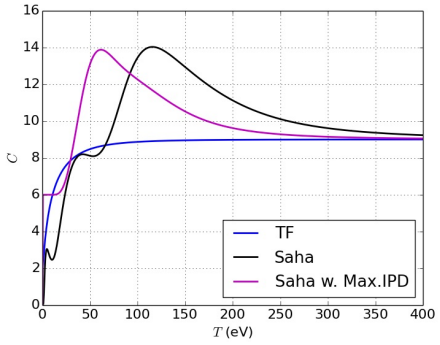

FIG. 5. Plot of the Specific Heat Capacity in terms of C as predicted by the Saha model with uniform application of the Ion Sphere IPD.

The resulting SHC curve is plotted in fig. 5. Since a uniform IPD of 97eV eliminates the first *four* ionization states, this only models the ionization of the two 1s electrons of carbon. Nonetheless, it is clear that the large maximum present in the full classical Saha model is due to these two innermost electrons. The position and magnitude of this maximum is a function of the ionization energies of the two innermost electrons.

The extent to which we trust the accuracy of the TF model, at least above 50eV, therefore appears to primarily depend on what we conclude about the 1s electrons

in this solid-density carbon plasma. Since the Ion Sphere model predicts a maximum IPD that is only a fraction of the isolated atom ionization energies (392 and 490eV respectively), we have to conclude that these states will still exist, and only be lowered by 97eV at most. This means that the magenta curve (Saha with Maximum IPD) in fig. 5 represents the most minimal effect of the 1s electrons that we can reasonably justify. The role of the 1s states can be verified by recalcuating the Saha SHC curve, but by artificially setting the ionization energies of the 1s electrons to very low values. In fig. 6 the curve resulting from setting these ionization energies to 25 and 50eV is shown. In fig. 6 we see that the magenta curve is now in good agreement with the TF curve for temperatures above 50eV.

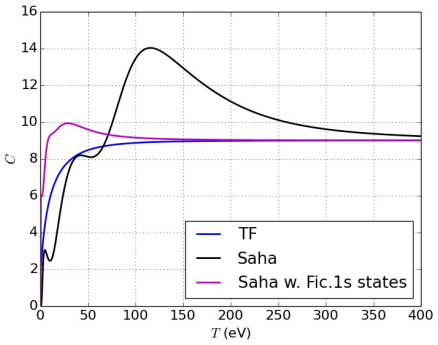

FIG. 6. Plot of the Specific Heat Capacity in terms of C as predicted by the Saha model with only the final two ionization stages with ionization energies set to 25 and 50eV.

So the TF and Saha models can be brought into rough agreement, but this requires that the 1s electrons experience an IPD which is very much greater than can be justified by the basic models of IPD. This problem exists at temperatures where quantum statistical issues should not have a significant impact on the SHC, so it must therefore be concluded that there are serious questions about the reliability of the TF SHC.

III. THERMODYNAMIC MODEL FOR THE SHC

In order to try and resolve the questions raised by the analysis presented in the preceding section we have developed an alternative method for calculating the electronic SHC. This is heavily based on the 'Partially Ionized Plasma' (PIP) model of Redmer[34,35] and similar 'thermodynamic' models for EOS that have been developed by other researchers[36–38]. Central to these approaches is using theoretical models for the contributions to the free energy to calculate the total free energy of the system. Once this is done, the required thermodynamic parameter, e.g. pressure, internal energy, or entropy, can then be determined using the appropriate thermodynamic differential relation.

Since we are principally interested in the behaviour at relatively high temperature we considered the following contributions to the free energy: the ideal free energy due to the free electrons, i.e.

$$F_{id,e} = N_e k_B T \left(\xi - \frac{2}{3} \frac{I_{3/2}(\xi)}{I_{1/2}(\xi)} \right), \tag{2}$$

where $\xi = \mu / k_B T$, and μ is the ideal chemical potential of the free electrons. By using this expression we are treating the free electrons as partially degenerate. We also account for the contribution due to the internal energy of atoms and ions, i.e.

$$F_{int} = -k_B T \sum_k N_k \ln Z_k^{int.}, \tag{3}$$

where,

$$Z_k^{int.} = g_k \exp\left(-\frac{\varepsilon_k}{k_B T} \right), \tag{4}$$

with the sum over k denoting the sum over ionization states, and g_k being the degeneracy of the ground state of the k-th ionization state, and ε_k being its ionization energy. We have also accounted for non-ideal contributions to the Free energy due to Coulomb interactions, via the results of Stolzmann and Blöcker[39]. In order to compute the free energy, one requires the plasma composition (population of the different ionization states). For this we have used the COMPTRA04 code to calculate the plasma composition at a given temperature and density[40]. Once the free energy is obtained the internal energy and SHC can then be calculated via,

$$U = F - \left(\frac{\partial F}{\partial T} \right)_V, \tag{5}$$

where U is the electronic internal energy.

One calculation was carried out for carbon at 2 gcm^{-3}. The results of this are shown in fig.7. As before we plot the SHC in terms of C where the SHC is expressed as Cen_i. We therefore expect $C \to 9$ at high temperature. In these, two versions of the thermodynamic calculation were performed: in model A we did not include the (Stolzmann-Blöcker) Coulomb corrections to the free energy, but these are included in model B.

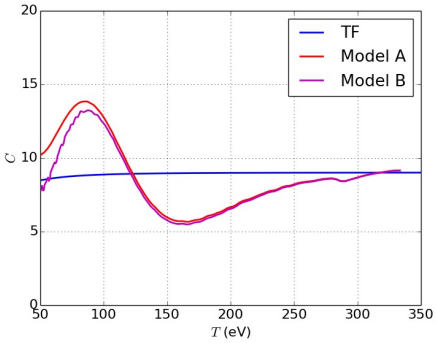

FIG. 7. Plot of the Specific Heat Capacity in terms of C as predicted by thermodynamic model for carbon at 2 gcm^{-3} in the 50–400eV range. For models see text. Note that we expect that $C \to 9$ at high temperatures.

Fig. 7 shows that both versions of the thermodynamic calculation show large deviations from the TF model as the previous analysis had suggested may be the case. Importantly, at low temperatures the SHC can be significantly larger than would be expected with the TF model. We have also carried out similar calculations for Al. The results of this calculation (with and without the contribution from the atom/ion internal energy), and its comparison to the TF model, is shown in fig. 8. Note that, for Al, we expect $C \to 19.5$ at high temperature.

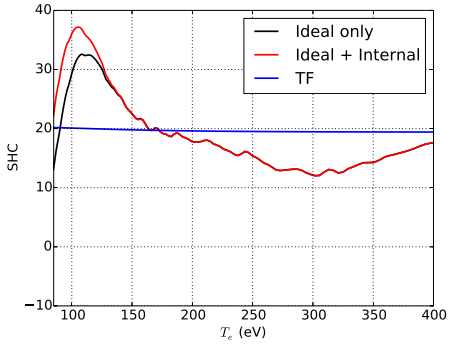

FIG. 8. Plot of the Specific Heat Capacity in terms of C as predicted by thermodynamic model for Al at 2.7gcm^{-3} in the 75–400eV range. For models see text. Note that we expect that $C \to 19.5$ at high temperature.

In the case of Al similar strong deviations from the TF model prediction are found. Interestingly the largest driver for these deviations appears to come from the ideal free energy of the electrons and how the degree of ionization changes with temperature. If the 'ideal free energy only' calculation is repeated with the TF ionization curve then the TF prediction is reproduced. Irrespective of the details, more advanced models have led us to the same conclusion: that the TF model is not a very accurate model for the SHC in problems relevant to laser-driven fast electron transport. Were these deviations confined to 5% or even 10% the importance could be questionable, however the deviations are found to reach 40–50%

IV. NUMERICAL SIMULATIONS

As the analysis in the preceding sections added considerable weight to the argument that the TF model is unlikely to be a good predictor of the electronic SHC for fast electron transport problems, we carried out a number of hybrid simulations to determine how much of a difference this makes to model calculations. A number of 3-D calculations were carried out using the KLYTEMNESTRA code, a code which is similar in many respects to the ZEPHYROS code[12,24].

These calculations are carried out using a 200×200×200 grid with a cell size of 0.5 μm in each direction. The fast electron injection modelled laser irradiation over a Gaussian spot with a characteristic radius of 5 μm, an intensity of 2×10^{19} Wcm^{-2}, a pulse duration of 500 fs. The fast electron distribution is an exponential distribution, with the characteristic temperature set to that given by Wilk's scaling[1], T_f = 1.5 MeV. The angular distribution used is a uniform distribution up to a cut-off half-angle, θ_{div}. This is varied over our simulation sets.

The target is uniform in composition and consisted of Al at 2.7 gcm^{-3}. The initial temperature is set to 80eV everywhere. The resistivity model used is the Spitzer resistivity throughout. In one simulation set (set A) the curve shown in fig. 8 is used for the SHC (Thermodynamic-COMPTRA Model), and in another set (set B) the TF prediction for the SHC is incorporated. A parameter scan is then carried out using multiple simulations, with θ_{div} varying from 23° to 52°.

V. RESULTS AND DISCUSSION

The main result that emerge from comparison of the TF simulation set to the Thermodynamic-COMPTRA set is that there are significant differences in the magnitude of the magnetic fields developed in the two cases. In table I the maximum value of B_z obtained along the line defined by z =0, x =12.5μm is shown for each simulation. This table also indicates the value of θ_{div} employed.

From table I it can be seen that the maximum value of B_z found along this line is consistently higher in the simulations using the Thermodynamic-COMPTRA model

θ_{div}	Th.-C. Sim.	max. B_z* (T)	TF Sim.	max. B_z* (T)
0.9	A1	2420	B1	1118
0.8	A2	2286	B2	1261
0.6	A3	2372	B3	1267
0.4	A4	2610	B4	1482

TABLE I. Summary of simulations and maximum value of B_z obtained on *z =0, x =12.5μm in Tesla.

than those that used the TF model for the SHC. This can readily be attributed to the higher SHC in the former at low temperatures. The percentage difference between the two ranges from 116% to 76%, so the difference in this crucial aspect of the simulation is really quite substantial. In all of the simulations, this region of the simulation is not subject to any significant filamentation, so comparison between the two sets is reasonable.

In terms of the other aspects of the simulation some caution needs to be applied because of the occurence of strong filamentation in these simulations which makes comparison between the two sets difficult. However in simulations A4 and B4, the beam remains quite collimated throughout. In this case, it is found that there are substantial differences in the electron temperature profiles (20% to 50%). This is shown in fig.s 9–11.

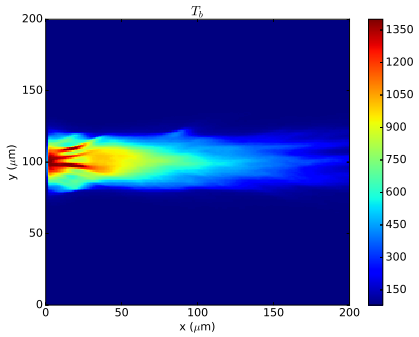

FIG. 9. Plot of the background electron temperature in run A4 in z =100μm mid-plane at 1ps.

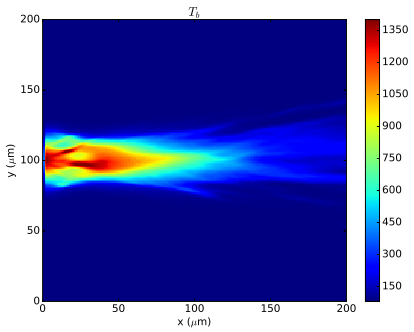

FIG. 10. Plot of the background electron temperature in run B4 in z =100μm mid-plane at 1ps.

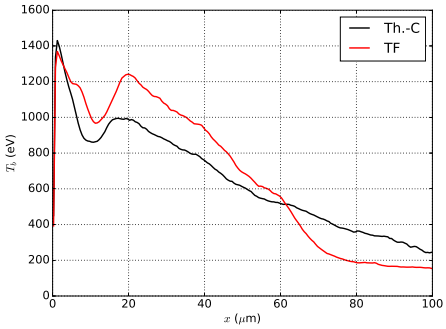

FIG. 11. Plot of the background electron temperature in runs A4 and B4 along the line $y = z$ =100μm at 1ps.

Fig.s 9–11 indicate that the TF model predicts a higher temperature at small to medium depths, but lower temperatures at large distances, with fig. 11 showing how substantial these discrepancies can be. Obviously this would have quite significant implications for potential experimental observables. A number of factors affect the temperature profiles in these plots. The differences in the SHC model is one matter, but the enhancement in the magnetic field growth (in the Thermodynamic-COMPTRA model) has a subtle effect on the fast electron flow, and this feeds back onto the temperature profile strongly as the Ohmic heating is quadratically sensitive to the fast electron current density.

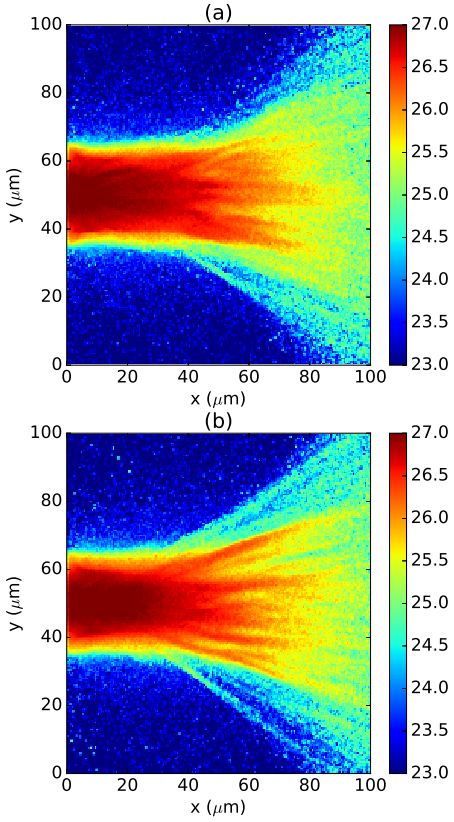

FIG. 12. Plot of the fast electron density at 500fs in runs (a) A3, and (b) B3. Units are $\log_{10}$ of n_f in m^{-3}.

We also observe subtle differences in the fast electron transport pattern. For example we find that the runs in set A tend to be somewhat more collimated than the corresponding run in set B. This follows naturally from set A having significantly higher magnetic flux densities in the large-scale collimating field. Fig. 12 shows plots of the fast electron density at 500fs in runs A3 and B3. It can be seen that the flow in run A3 is somewhat better collimated than that in run B3. So there can also be significant implications for any experimental observables that would depend on the fast-electron transport pattern.

In summary, we find that there are quite significant differences between the two simulation sets, which only differ in terms of the SHC model that they employ. The largest difference is in the magnetic field generation (a factor of two) but there are significant differences in background electron temerature and the flow pattern of the fast electrons. Overall we can conclude that moving from the TF model (which we have argued has unrealistic features) to a model which is more realistic leads to substantial changes, and ones that could have a considerable effect on the interpretation of experiments.

VI. CONCLUSIONS

In this paper we have argued that the Thomas-Fermi (TF) model is unlikely to be a particularly good model for the electronic specific heat capacity (SHC) of solids in laser-generated fast electron transport problems, particularly in low to intermediate- Z materials. The most worrying concern that we raised was that there could be serious discrepancies at relatively high temperatures (i.e. around 100eV) which could arise due to the TF model not accounting for any quantum shell structure, and that accounting for Ionization Potential Depression would not necessarily remove any such discrepancies. To illustrate this concern we compared the prediction of a simple Saha-based model to the TF model. For the sake of clarity, we only expect these discrepancies to be pronounced at about 100eV, as the effect here concerns the core electrons, and thus we do not expect this to affect very low temperatures.

We then proceeded to validate this concern by developing a more sophisticated model for the SHC by using a Thermodynamic approach and the COMPTRA04 code[40] to calculate the plasma composition at a given temperature. The SHC curves obtained from this approach validate our concerns, showing serious deviations from the TF prediction. These deviations can be up to 40–50% over substantial temperature ranges. In some cases, such as that of solid carbon, the deviations appear to originate from the TF model neglecting quantum shell structure. In other cases the major contribution to the deviation most likely comes from differing calculations of the plasma composition (as is the case for Al). Irrespective of the precise cause, these deviations are of such a magnitude that it seems rather unlikely that they are negligible.

When we analyzed the impact the aforementioned discrepancies had on a set of model fast electron transport calculations we have found that the differences in the SHC lead to significant differences in key aspects of the simulation results. The starkest of these is in the magnetic field, where differences of a factor of two were routinely obtained for the magnetic flux density. There are also significant differences in the background temperature and the fast electron propagation pattern. We can therefore confidently conclude that using more sophisticated SHC models is likely to have a significant impact

on the use of computer models to interpret fast electron transport experiments. One avenue of future work will be to re-examine current and extant experimental observations[41–45] in light of the study reported herein.

The data that support the findings of this study are available from the corresponding author upon reasonable request.

ACKNOWLEDGEMENTS

APLR is grateful for computing resources provided by STFC Scientific Computing Department's SCARF cluster.

Appendix A: Classical Saha

The 'classical' Saha equation can be derived from expressions for the chemical potential that assume ideal (non-interacting) non-degenerate, non-relativistic electron and ion species. This leads to a set of equations for the number density of each ionization state,

$$\frac{n_e n_{k+1}}{n_k} = \frac{2}{\Lambda_{e,th}^3}\frac{G_{k+1}}{G_k}\exp(-I_k/k_B T), \tag{A1}$$

where G_k is the internal partition function, I_k is the ionization energy of the k-th state, and $\Lambda_{e,th}$ is the thermal wavelength of the electrons. As this is an ideal system, the *electron* internal energy can then be expressed as,

$$U_e = \frac{3}{2}Z^\star e n_0 T_e + \sum_k e n_k I_k, \tag{A2}$$

where $n_0 = \sum_k n_k$. By solving the Saha equations numerically one can thus determine $U_e = U_e(T)$ (at a given n_0) and thus the electronic SHC can be computed numerically by taking the temperature derivative.

[1] S. C. Wilks, W. L. Kruer, M. Tabak, and A. B. Langdon, Phys. Rev. Lett. **69**, 1383 (1992).
[2] S. P. Hatchett, C. G. Brown, T. E. Cowan, E. A. Henry, J. S. Johnson, M. H. Key, J. A. Koch, A. B. Langdon, B. F. Lasinski, R. W. Lee, A. J. Mackinnon, D. M. Pennington, M. D. Perry, T. W. Phillips, M. Roth, T. C. Sangster, M. S. Singh, R. A. Snavely, M. A. Stoyer, S. C. Wilks, and K. Yasuike, Physics of Plasmas **7**, 2076 (2000).
[3] M. Sherlock, Physics of Plasmas **16**, 103101 (2009).
[4] F. N. Beg, A. R. Bell, A. E. Dangor, C. N. Danson, A. P. Fews, M. E. Glinsky, B. A. Hammel, P. Lee, P. A. Norreys, and M. Tatarakis, Physics of Plasmas **4**, 447 (1997).
[5] M.Tabak, J.Hammer, M.E.Glinksy, W.L.Kruer, S.C.Wilks, J.Woodworth, E. M. Campbell, M.D.Perry, and R.J.Mason, Phys.Plasmas **1** (1994).
[6] M.Tabak, D.S.Clark, S.P.Hatchett, M.H.Key, B.F.Lasinski, R.A.Snavely, S.C.Wilks, R.P.J.Town, R.Stephens, E.M.Campbell, R.Kodama, K.Mima, K.A.Tanaka, S.AtzenS.Atzeni, and R.Freeman, Phys.Plasmas **\bf 12**, 057305 (2005).
[7] A.P.L.Robinson, D.J.Strozzi, J.R.Davies, L.Gremillet, J.J.Honrubia, T.Johzaki, R.J.Kingham, M.Sherlock, and A.A.Solodov, Nuclear Fusion **54**, 054003 (2014).
[8] S. Atzeni, A. Schiavi, J. J. Honrubia, X. Ribeyre, G. Schurtz, P. Nicolai, M. Olazabal-Loume, C. Bellei, R. G. Evans, and J. R. Davies, Physics of Plasmas **15**, 056311 (2008).
[9] P.McKenna, A.P.L.Robinson, D.Neely, M.P.Desjarlais, D.C.Carroll, M.N.Quinn, X.H.Yuan, C.M.Brenner, M.Burza, M.Coury, P.Gallegos, R.J.Gray, K.L.Lancaster, Y.T.Li, X.X.Lin, O.Tresca, and C.-G.Wahlström, Phys.Rev.Lett. **106**, 185004 (2011).
[10] T.G.White, N.J.Hartley, B.Borm, B.J.B.Crowley, J.W.O.J.W.O.Harris, D.C.Hochhaus, T.Kaempfer, K.Li, P.Neumayer, L.K.Pattison, F.Pfeifer, S.Richardson, A.P.L.A.P.L.Robinson, I.Uschmann, and G.Gregori, Phys. Rev. Lett. **112**, 145005 (2014).
[11] D.A.MacLellan, D.C.Carroll, R.J.Gray, N.Booth, M.Burza, M.P.Desjarlais, F.Du, B.Gonzalez-Izquierdo, D.Neely, H.W.Powell, A.P.L.Robinson, D.R.Rusby, G.G.Scott, X.H.Yuan, C.-G.Wahlström, and P.McKenna, Phys.Rev.Lett. **111**, 095001 (2013).
[12] A.P.L.Robinson, H.Schmitz, and J.Pasley, Phys.Plasmas **20**, 122701 (2013).
[13] K. L. Lancaster, A. P. L. Robinson, J. Pasley, P. Hakel, T. Ma, K. Highbarger, F. N. Beg, S. N. Chen, R. L. Daskalova, R. R. Freeman, J. S. Green, H. Habara, P. Jaanimagi, M. H. Key, J. King, R. Kodama, K. Krushelnick, H. Nakamura, M. Nakatsutsumi, A. J. MacKinnon, A. G. MacPhee, R. B. Stephens, L. Van Woerkom, and P. A. Norreys, Physics of Plasmas **24**, 083115 (2017), publisher: American Institute of Physics.
[14] J.J.Honrubia and others, Las.Part.Beams **24**, 217 (2006).
[15] A.Debayle, J.J.Honrubia, E.d'Humieres, and V.T.Tikhonchuk, Phys. Rev. E **82**, 036405 (2010).
[16] X. H. Yuan, A. P. L. Robinson, M. N. Quinn, D. C. Carroll, M. Borghesi, R. J. Clarke, R. G. Evans, J. Fuchs, P. Gallegos, L. Lancia, D. Neely, K. Quinn, L. Romagnani, G. Sarri, P. A. Wilson, and P. McKenna, New Journal of Physics **12**, 063018 (2010).
[17] A.R.Bell and R.J.Kingham, Phys.Rev.Lett. **91**, 035003 (2003).
[18] J.J.Honrubia and J.Meyer-ter-Vehn, Nucl.Fusion **46**, L25 (2006).
[19] H.Schmitz, R.Lloyd, and R.G.Evans, Plasma Phys.Control.Fusion **54**, 085016 (2012).
[20] F.Perez, A.Debayle, J.Honrubia, M.Koenig, D.Batani, S.D.Baton, F.N.Beg, C.Benedtti, E.Brambrink, S.Chawla, F.Dorchies, C.Fourment, M.Galimberti, L.A.Gizzi, L.Gremillet, R.Heathcote, D.P.Higginson, S.Hulin, R.Jafer, P.Koester, L.Labate, K.L.Lancaster, A.J.MacKinnon, A.G.MacPhee, W.Nazarov, P.Nicolai, J.Pasley, R.Ramis, M.Richetta, J.J.Santos, A.Sgattoni, C.Spindloe, B.Vauzour, T.Vinci, and L.Volpe, Phys.Rev.Lett. **107**, 065004 (2011).
[21] A.P.L.Robinson, H.Schmitz, J.S.Green, C.P.Ridgers, and N.Booth, Plasma Phys. and Control. Fusion **57**, 064004 (2015).
[22] A.P.L.Robinson and M.Sherlock, Phys.Plasmas **14**, 083105 (2007).
[23] A.P.L.Robinson, M.Sherlock, and P.A.Norreys, Phys.Rev.Lett. **100**, 025002 (2008).
[24] A.P.L.Robinson, M.H.Key, and M.Tabak, Phys.Rev.Lett. **108**, 125004 (2012).
[25] B.Ramakrishna, S.Kar, A.P.L.Robinson, D.J.Adams, K.Markey, M.N.Quinn, X.H.Yuan, P.McKenna, K.L.Lancaster, J.S.Green, R.H.H.Scott, P.A.Norreys, J.Schreiber, and M.Zepf, Phys.Rev.Lett. **105**, 135001 (2010).
[26] S. Atzeni and J. Meyer-ter Vehn, *The Physics of Inertial Fusion: BeamPlasma Interaction, Hydrodynamics, Hot Dense Matter* (OUP Oxford, 2004).
[27] D.J.Hoarty, P.Allan, S.F.James, C. R. D. Brown, L.M.R.Hobbs, M.P.Hill, J.W.O.Harris, J.Morton, M.G.Brookes, R.Shepherd, J.Dunn, H.Chen, E. V. Marley, P.Beiersdorfer, H.K.Chung, R.W.Lee, G.Brown, and J.Emig, Phys.Rev.Lett. **110**, 265003 (2013).

[28]D. Salzmann, *Atomic Physics in Hot Plasmas* (Oxford University Press, 1998).
[29]D. Sheppard, J. D. Kress, S. Crockett, L. A. Collins, and M. P. Desjarlais, Physical Review E **90**, 063314 (2014), publisher: American Physical Society.
[30]M. Das and S. V. G. Menon, Physical Review B **79**, 045126 (2009), publisher: American Physical Society.
[31]J. C. Pain, High Energy Density Physics Radiative Properties of Hot Dense Matter, **3**, 204 (2007).
[32]B. F. Rozsnyai, High Energy Density Physics **8**, 88 (2012).
[33]B. Ritchie, Physics of Plasmas **11**, 3417 (2004), publisher: American Institute of Physics.
[34]R. Redmer, Physical Review E **59**, 1073 (1999), publisher: American Physical Society.
[35]S. Kuhlbrodt and R. Redmer, Physical Review E **62**, 7191 (2000), publisher: American Physical Society.
[36]Q. Chen, Y. Zhang, L. Cai, Y. Gu, and F. Jing, Physics of Plasmas **14**, 012703 (2007), publisher: American Institute of Physics.
[37]K. Wang, Z. Shi, Y. Shi, J. Bai, J. Wu, and S. Jia, Physics of Plasmas **22**, 062709 (2015), publisher: American Institute of Physics.
[38]M. T. Gabdullin, T. S. Ramazanov, R. Redmer, and G. B. Akhtanova, Contributions to Plasma Physics **53**, 311 (2013), _eprint: https://onlinelibrary.wiley.com/doi/pdf/10.1002/ctpp.201200127.
[39]W. Stolzmann and T. Blöcker, Physics Letters A **221**, 99 (1996).
[40]S. Kuhlbrodt, B. Holst, and R. Redmer, Contributions to Plasma Physics **45**, 73 (2005), _eprint: https://onlinelibrary.wiley.com/doi/pdf/10.1002/ctpp.200510009.
[41]D.Batani, A. Antonicci, F. Pisani, T. A. Hall, D. Scott, F. Amiranoff, M. Koenig, L. Gremillet, S. Baton, E. Martinolli, C. Rousseaux, and W. Nazarov, Phys.Rev.E **65**, 066409 (2002).
[42]E. Martinolli, M. Koenig, F. Amiranoff, S. D. Baton, L. Gremillet, J. J. Santos, T. A. Hall, M. Rabec-Le-Gloahec, C. Rousseau, and D. Batani, Phys.Rev.E **70**, 055402(R) (2004).
[43]E. Martinolli, M. Koenig, S. D. Baton, J. J. Santos, F. Amiranoff, D. Batani, E. Perelli-Cippo, F. Scianitti, L. Gremillet, R. Mélizzi, A. Decoster, C. Rousseaux, T. A. Hall, M. H. Key, R. Snavely, A. J. MacKinnon, R. R. Freeman, J. A. King, R. Stephens, D. Neely, and R. J. Clarke, Phys.Rev.E **73**, 046402 (2006).
[44]B. Vauzour, J. J. Santos, A. Debayle, S. Hulin, H.-P. Schlenvoigt, X. Vaisseau, D. Batani, S. D. Baton, J. J. Honrubia, P. Nicolaï, F. N. Beg, R. Benocci, S. Chawla, M. Coury, F. Dorchies, C. Fourment, E. d'Humières, L. C. Jarrot, P. McKenna, Y. J. Rhee, V. T. Tikhonchuk, L. Volpe, and V. Yahia, Phys.Rev.Lett. **109**, 255002 (2012).
[45]X. Vaisseau, A. Debayle, J. Honrubia, S. Hulin, A. Morace, P. Nicolaï, H. Sawada, B. Vauzour, D. Batani, F. Beg, J. Davies, R. Fedosejevs, R. Gray, G. Kemp, S. Kerr, K. Li, A. Link, P. McKenna, H. McLean, M. Mo, P. Patel, J. Park, J. Peebles, Y. Rhee, A. Sorokovikova, V. Tikhonchuk, L. Volpe, M. Wei, and J. Santos1, Phys.Rev.Lett. **114**, 095004 (2015).

PLEASE CITE THIS ARTICLE AS DOI: 10.1063/5.0007357

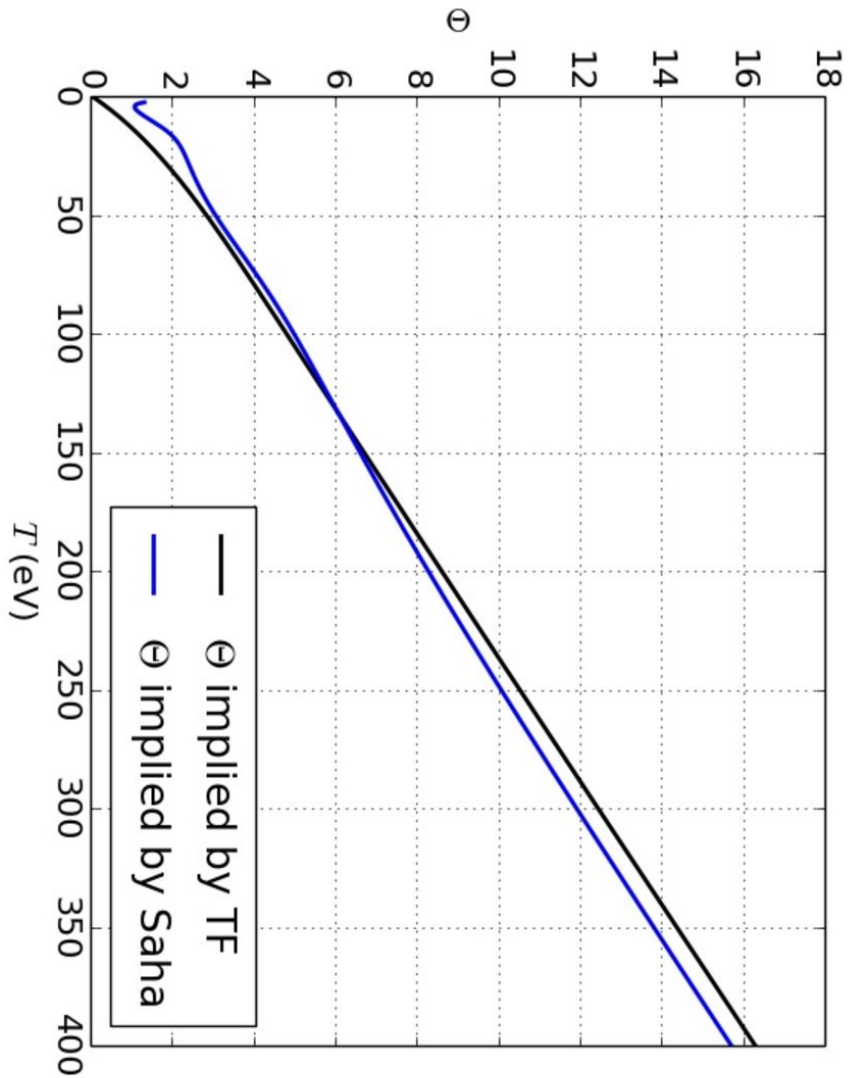

PLEASE CITE THIS ARTICLE AS DOI: 10.1063/5.0007357

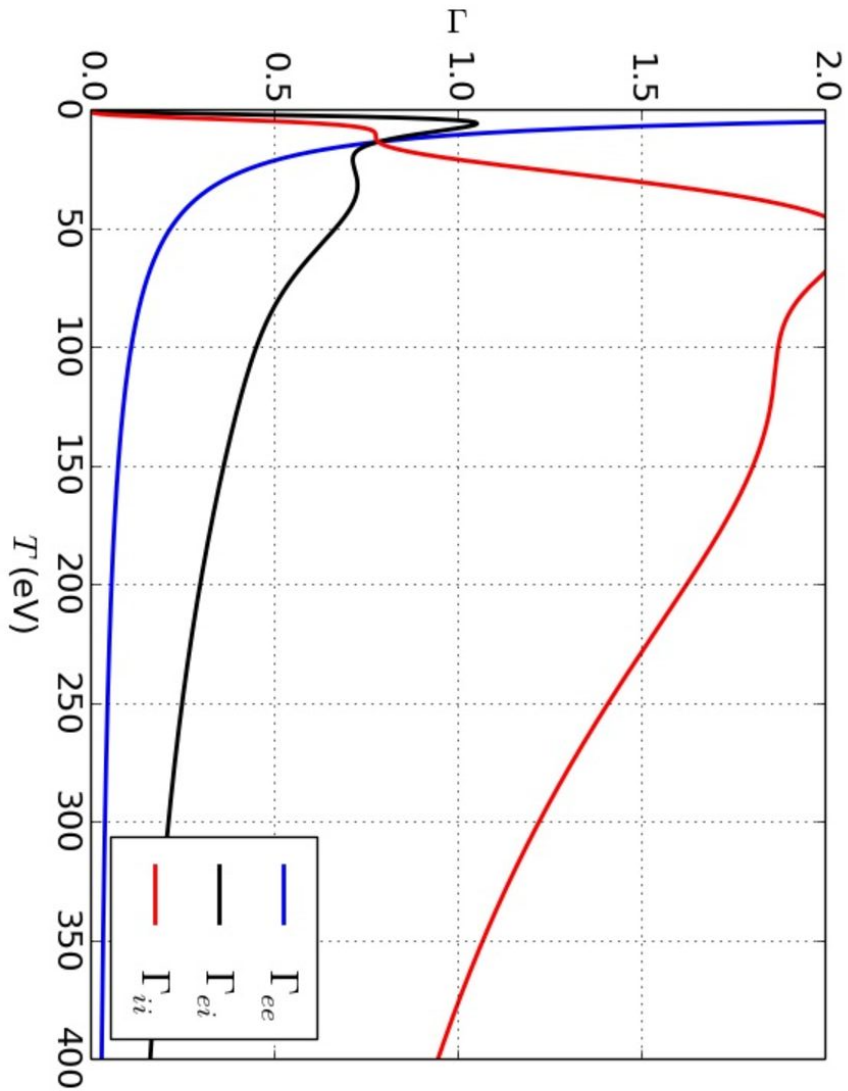

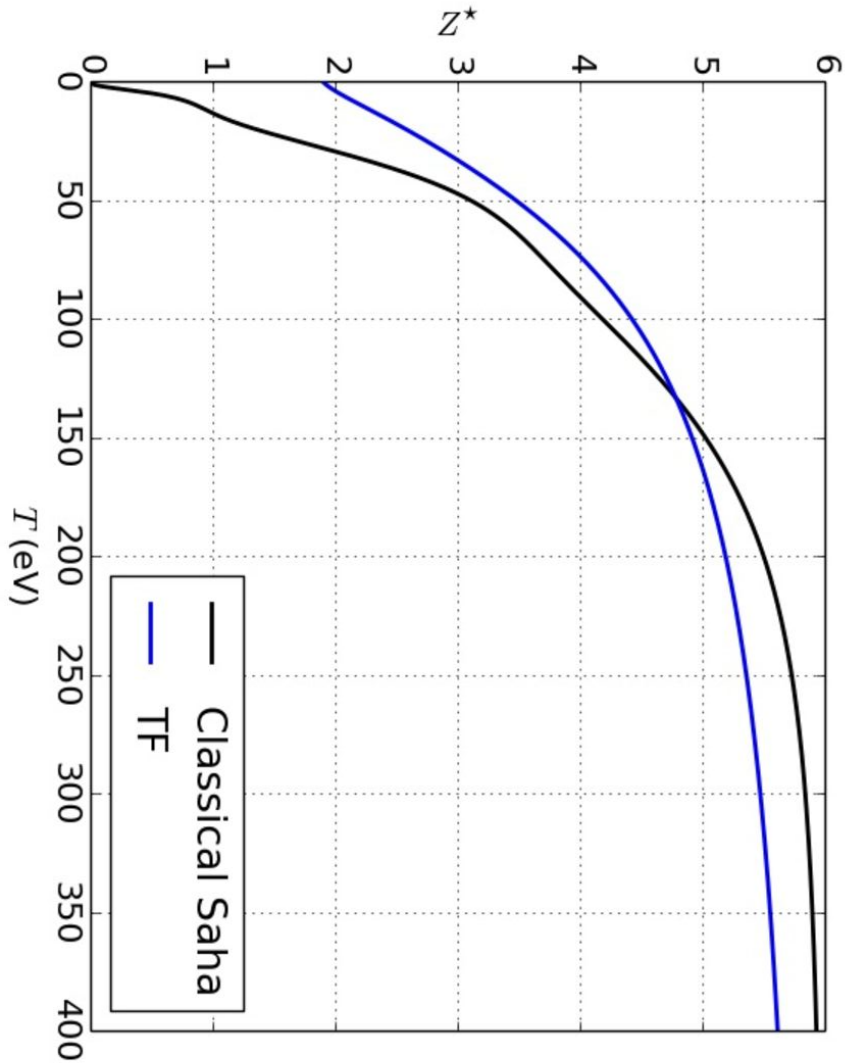

PLEASE CITE THIS ARTICLE AS DOI: 10.1063/5.0007357

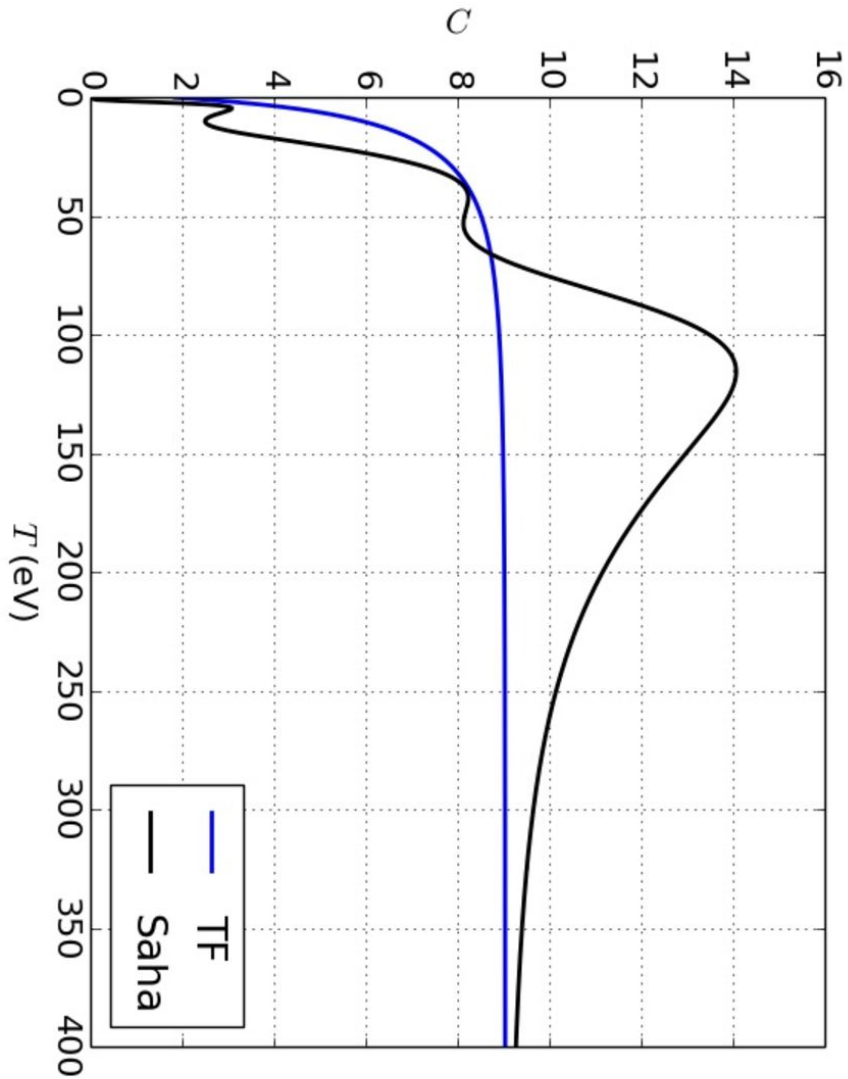

PLEASE CITE THIS ARTICLE AS DOI: 10.1063/5.0007357